Synthesis of Nanocrystalline TiO₂ by Sol-Gel Combustion Hybrid Method and Its Application to Dye Solar Cells

Chi-Hwan Han,[*] Hak-Soo Lee, and Sang-Do Han

Electrical & Electronic Materials Research Center, Korea Institute of Energy Research, Daejeon 305-343, Korea
[*]E-mail: hanchi@kier.re.kr

TiO₂ nanopowders were synthesized by new sol-gel combustion hybrid method using acetylene black as a fuel. The dried gels exhibited autocatalytic combustion behaviour. TiO₂ nanopowders with an anatase structure and a narrow size distribution were obtained at 400-600 ^{o}C. Their crystal structures were examined by powder X-ray diffraction (XRD) and their morphology and crystal size were investigated by scanning electron microscopy (SEM). The crystal size of the nanopowders was found to be in the range of 15-20 nm. TiO₂ powders synthesized at 500 ^{o}C and 600 ^{o}C were applied to a dye solar cell. An efficiency of 5.2% for the conversion of solar energy to electricity ($J_{sc} = 11.79$ mA/cm^2, $V_{oc} = 0.73$ V, and $FF = 0.58$) was obtained for an AM 1.5 irradiation (100 mW/cm^2) using the TiO₂ nanopowder synthesized by the sol-gel combustion hybrid method at 500 ^{o}C.

Key Words : Nanocrystalline TiO₂, Sol-gel combustion hybrid method, Dye solar cell, Ru-complex

Introduction

TiO₂ has been widely used in various devices such as dye-sensitized solar cells (DSCs), photocatalysts, photochromic glasses, gas sensors, and for applications such as self-cleaning of windows.[1-6] After years of evolutionary research on the production of TiO₂ nanopowder, many technologies that are based on build-up processes such as the gas phase process, liquid phase process, and solid phase process have been practically developed.[7,8] In most cases, TiO₂ powder is synthesized through gas-phase reactions such as the combustion of titanium tetrachloride,[9,10] and liquid-phase reactions such as the precipitation of titanium hydroxide followed by calcination.[11,12] The gas-phase process yields fine well-crystallized particles; however, the reproducibility of this process is low due to its complicated mechanism. The liquid-phase process is simple and can also be carried out in laboratories; however, its drawbacks are that it needs a large amount of organic materials and it is difficult to obtain particles with both a large surface area and high crystallinity.[13,14] Therefore, there is a need to develop a simple and efficient method to obtain TiO₂ nanoparticles with a narrow size distribution and high crystallinity.

Sol-gel combustion is a novel method that uses a unique combination of the chemical sol-gel process and combustion. The sol-gel synthesis of ceramic oxides offers advantages such as high purity, good homogeneity, and low processing temperature.[15,16] Combustion synthesis offers advantages such as low energy requirements, simple equipment, and a short operation time because it uses a sustainable exothermic solid-solid reaction among the raw materials.[17] The sol-gel combustion method is based on the gelling and subsequent combustion of an aqueous solution containing salts of the desired metals and an inorganic fuel such as acetylene black, and it yields a voluminous and fluffy product with a large surface area. This process has the advantages of inexpensive precursors, a simple preparation method, and the ability to yield nanosized powders.[18]

In the present study, nano-crystallized TiO₂ powders were synthesized by the sol-gel combustion hybrid method using acetylene black as a fuel. The possibility of the application of these powders to DSCs was also investigated.

Experimental

Synthesis of nanocrystalline TiO₂ powder. Titanium isopropoxide was purchased from Aldrich and was used as a starting material. Acetylene black was purchased from the Chevron Phillips Chemical Company. Figure 1 shows the flow scheme of the combustion process used for the synthesis of nanocrystalline TiO₂ powder.

First, 7 mL of titanium isopropoxide was dissolved in 20 mL of isopropanol and 0.4 g of acetylene black was added to the titanium solution followed by an aqueous NH₄OH solution dropwise under constant stirring until it was transformed into a sol at ambient conditions. The sol was heated at 120 ^{o}C to obtain a dry gel. The gel was ignited in air at 400-700 ^{o}C, resulting in an auto-combustion process that yielded TiO₂ powders.

The TiO₂ nanopowders were examined by powder X-ray diffraction (XRD; Rigaku, Ultima Plus diffractometer D/Max 2000). The morphology and size of the particle were investigated by using a field emission scanning electron microscope (FE-SEM; Hitachi, S-4300). Thermal analysis was carried out using a simultaneous thermal analyzer (STA; Scinco, STA S-1500) with a heating rate of 5 ^{o}C/min. The BET surface area of each sensor material was measured by the nitrogen sorption method at the liquid nitrogen temperature using Micromeritics ASAP 2010. Before each measurement, the samples were degassed at 200 ^{o}C in vacuum until a
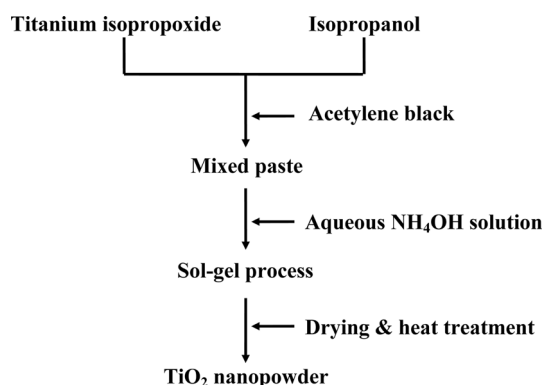
Titanium isopropoxide   **Isopropanol**

←— **Acetylene black**

Mixed paste

←— **Aqueous NH₄OH solution**

Sol-gel process

←— **Drying & heat treatment**

TiO₂ nanopowder

Figure 1. Process for synthesis of TiO₂ nanopowder.

constant pressure (~3 μmHg) was achieved. The infrared spectra were recorded using Fourier-transformed infrared spectrophotometer (FT/IR-610, JASCO) in diffused reflectance mode. UV-vis diffuse reflectance absorption spectra were measured using a UV-vis spectrophotometer (Lambda 2, Perkin Elmer) with reflectance spectroscopy accessory.

Preparation of TiO₂ photoelectrode and Ru(II) dye coating. The TiO₂ nanopowders were dispersed in ethanol using an ultrasonic horn. After sonification, the colloidal suspensions were concentrated using a rotary evaporator and transformed into a screen-printable paste by the addition of ethyl cellulose and terpineol. The TiO₂ paste was deposited onto conducting glass with a fluorine-doped stannic oxide layer (FTO, TEC 8/2.3 mm, 8 $\Omega/\square$, Pilkington) using a screen-printing method. The resulting layer was calcined for 2 h at 470 °C in a muffle furnace. This process was repeated three times until a thickness of 15 μm was obtained. The area of the prepared porous TiO₂ electrode was 25 mm² (5 mm × 5 mm). Dye absorption was carried out by dipping the TiO₂ electrode in a 4×10^{-4} M t-butanol/acetonitrile (Merck, 1:1) solution of N719 (Solaronix) for 48 h at 25 °C. The photoelectrode was then washed, dried, and immediately used to measure the performance of a solar cell.

Photovoltaic characterization. Transparent counter electrodes were prepared by placing a few drops of 10 mM hydrogen hexachloroplatinate (IV) hydrate (99.9%, Aldrich) and 2-propanol solution on FTO glass (TEC 8/2.3 mm, Pilkington) and calcining it for 2 h at 450 °C. The liquid electrolyte was composed of 0.70 M 1,2-dimethyl-3-propyl-imidazolium iodide (Sanko), 0.10 M LiI (Aldrich), 40 mM iodine (Aldrich), and 0.125 M 4-tert-butylpyridine (Aldrich) in acetonitrile. The photoelectrochemical properties of the prepared dye-sensitized solar cell were measured by using a computer-controlled digital source meter (Potentiostat/ Galvanostat Model 273A, EG & G) and a solar simulator (AM 1.5, 100 mW/cm², Driel) as a light source.

Results and Discussion

Synthesis process of TiO₂ nanopowders. When the dried gel was heat treated in a high form crucible the powder on the inner side of the crucible did not burn well and acetylene black remained unburnt. Hence, the dried gel was well

dispersed on a boat-type crucible and then heat treated in the muffle furnace.

The DSC/TGA plot of the products obtained by the combustion of the sample is shown in Figure 2. An endothermic peak was observed at 100 °C and four exothermic peaks were observed at 264 °C, 313 °C, 434 °C, and 538 °C. The endothermic peak at 100 °C can be attributed to the evaporation of the remaining solvent. The first two exothermic peaks at 264 °C and 313 °C may be attributed to the decomposition of the organic materials. The peaks at 434 °C and 538 °C could be attributed to the formation of the TiO₂ nanocrystals and the decomposition of acetylene black, respectively. Figure 3 shows colour images of the powders that were heat treated at 400-700 °C. The colour of the powder that was heat treated at 400 °C was grey, while that of all the powders that were heat treated above 500 °C was white. This was confirmed by running the UV-vis diffuse reflectance absorption spectra of the powders calcined at various temperatures between 400 °C and 700 °C (Figure 4). At 400 °C the material showed absorbance due to mixture of colours i.e black colour while at higher temperatures the synthesized material did not show any absorbance confirming thereby the white body colour of the material. Figure 5 shows the FT-IR spectra of the powders calcined at various temperatures between 400 °C and 700 °C confirming that the organic materials burnt out completely above 400 °C. The UV-vis diffuse reflectance absorption spectra also showed that the intensity of the absorption increaseds in ultra-violet region with the increase of tempera-
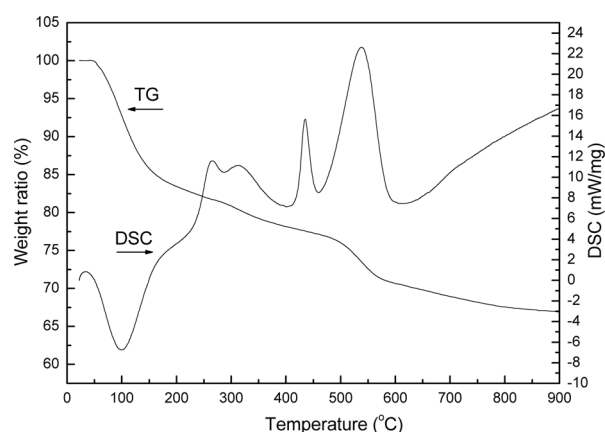
Figure 2. TG and DTA plots of the dried gel recorded between 30 and 900 °C at a heating rate of 5 °C/min.
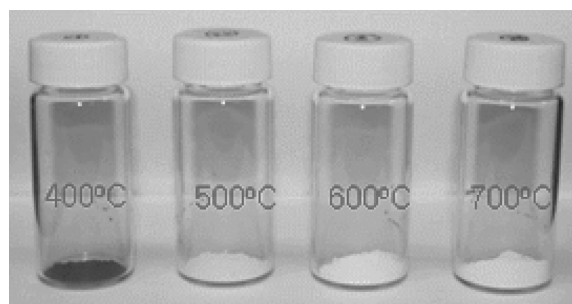
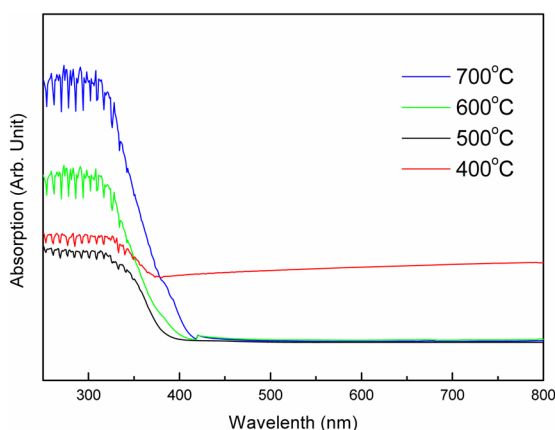**Figure 3**. Colours of the powders calcined at various temperatures between 400 and 700 °C.

Figure 4. UV-vis diffuse reflectance absorption spectra of the powders calcined at various temperatures between 400 °C and 700 °C.
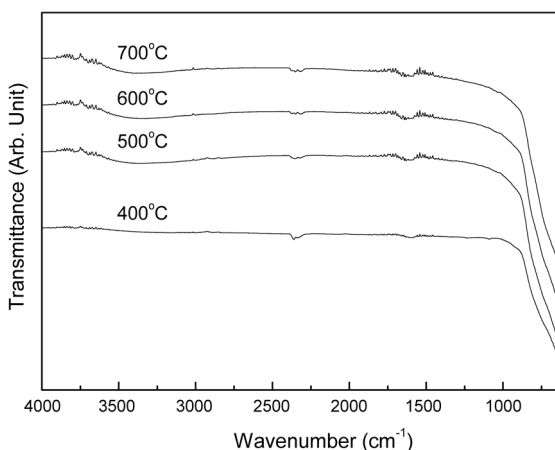

Figure 5. FT-IR spectra of the powders calcined at various temperatures between 400 °C and 700 °C.

ture due to increase in size of the particle.

The results of the XRD analysis of the powders that were heat treated at 400-700 °C are shown in Figure 6. The XRD patterns for the powders calcined at 400-500 °C showed the formation of pure TiO_2 with an anatase structure. The powder calcined at 600 °C also had an anatase structure but small amount of rutile structure was observed. However, the XRD pattern of the powder calcined at 700 °C showed the transformation of the anatase phase to the rutile phase completely. The intensity of the peaks of rutile phase increased with the calcination temperature.

Based on the results of the thermal analysis, colour change, and XRD data, it was found that the anatase structure of nano-crystalline TiO_2 was formed at around 400 °C while the anatase structure changed to the rutile structure around 700 °C, and the acetylene black burnt at around 500 °C.

Characterization of TiO₂ nanopowders. We used the scanning electron microscopy (SEM) to investigate the morphology of the TiO_2 powders. Figure 7 shows the SEM images of the powders. It is clearly observed that the morphology of the powders calcined below 600 °C is quite different from that of the powder calcined at 700 °C. The powders calcined below 600 °C have only nanosized particles, while in the
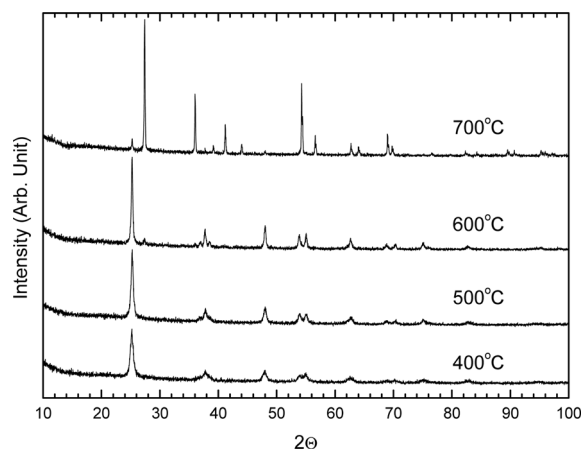

Figure 6. XRD results of the powders calcined at various temperatures between 400 °C and 700 °C.

powders calcined at 400 °C, particles with a size of 10 nm were agglomerated together with acetylene black. The size of the particles increased slightly with the increase of temperature upto 600 °C and remained evenly distributed with a size less than 20 nm. However, the powders calcined at 700 °C showed crystallinity with particle sizes varying between 20 nm and 200 nm.

Based on the XRD and SEM results, it can be inferred that acetylene black burnt slowly around 400 °C and prevented any increase in the crystal size of TiO_2 by releasing CO_2 gas. As acetylene black exhausted around 700 °C, an abrupt change in the crystal size and structural change from anatase to rutile were observed. The temperature of 600 °C is a very high temperature for the synthesis of nanopowders because the size of the particles increases at high temperatures. Using the sol-gel combustion hybrid method and acetylene black, we obtained highly crystallized nanoparticles with an anatase structure and a size of around 20 nm at 600 °C.

The BET surface areas were measured and are listed in Table 1. The sample heat treated at 400 °C had a high surface area of 365 m²/g. This may be explained by the fact that the remaining acetylene black had a high surface area. The samples heat treated at 500 °C and 600 °C had surface areas
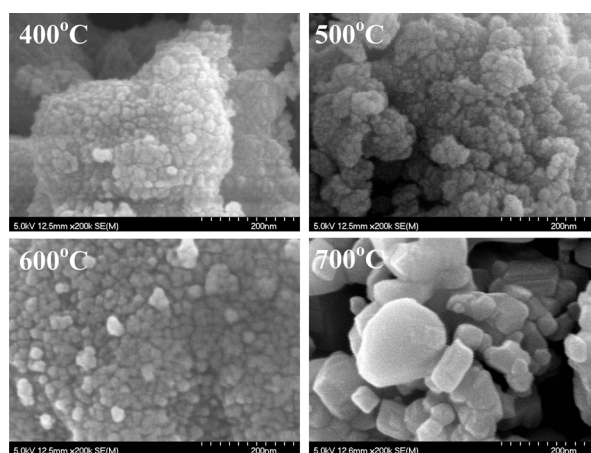

Figure 7. SEM images of the powders calcined at various temperatures between 400 and 700 °C.

Table 1. Particle sizes and BET surface areas of the powders synthesized by the sol-gel combustion hybrid method at various temperatures

	400 °C	500 °C	600 °C	700 °C
Surface area (m²/g)	365.8	242.7	97.6	5.9

of 242.7 m²/g and 97.5 m²/g, respectively. These surface areas are larger than those of traditional nanoparticles to some extent, which are normally between 50 m²/g and 120 m²/g.[19] The surface area decreased drastically as the heat treatment temperature increased; the sample that was calcined at 700 °C had a surface area of only 5.9 m²/g.

Application of the synthesized TiO$_2$ powder to DSC. The performance of the DSCs, developed using TiO$_2$ powders synthesized by the sol-gel combustion hybrid method and calcined at 500 °C and 600 °C was tested. Figure 8 shows the I-V characteristics of the cells.

A solar conversion efficiency of 5.02% was obtained for the powder calcined at 500 °C without sufficient optimization. The short-circuit photocurrent density (J_{sc}) and open-circuit photovoltage (V_{oc}) were 11.79 mA/cm² and 0.73 V, respectively. For the powder calcined at 600 °C, the values of the J_{sc} and V_{oc} were 6.54 mA/cm² and 0.77 V, respectively. The solar conversion efficiency of the powder calcined at 600 °C decreased to 2.86% because of the decrease in the surface area. As shown in Table 1, the surface area of the powder decreased with the increase in temperature. As may be seen, the powder calcined at 600 °C had a surface area of 97.6 m²/g only, while the powder calcined at 500 °C had a comparatively larger surface area of 242.7 m²/g. It was noted that when the synthesized TiO$_2$ powder was coated on the FTO glass and the Ru-dye was absorbed by the TiO$_2$ layer, the colours of the layer at 500 °C and 600 °C were red and pink, respectively. This implies that the powder calcined at 600 °C absorbed a lesser amount of dye in comparison to the powder calcined at 500 °C, thereby decresing the I_{sc} and
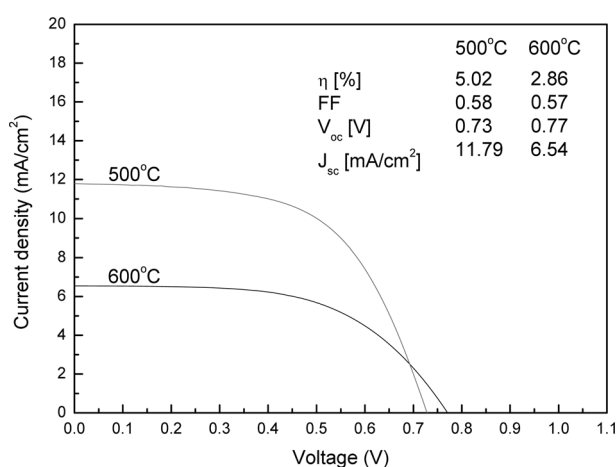
solar current efficiency of the developed cell. However, the V_{oc} of the powder calcined at 600 °C was 0.04 V, higher than that of the powder calcined at 500 °C. This may stem from a decrease in the free area of the photoelectrode prepared with TiO$_2$ that was calcined at 600 °C and exposed to a redox electrolyte. The decrease in the free area suppresses the dark current arising from the reduction of I$_3^-$ by conduction band electrons at the semiconductor-electrolyte junction.[20]

Conclusion

TiO$_2$ nanopowders were been synthesized by using a new sol-gel combustion hybrid method. Acetylene black was used as a fuel and to prevent increase in the size of the TiO$_2$ particles. The powder synthesized at 500 °C had particles with sizes of 15-20 nm and a BET surface area of 242.7 m²/g. A solar conversion efficiency of 5.02% was obtained. The sol-gel combustion hybrid method involves a low-temperature self-propagating ignition process, which is safe, simple, and fast, for the production of very fine homogeneous powders. Thus, this process offers a simple and effective route to the synthesis of uniform TiO$_2$ nanopowders, which can be used in dye-sensitized solar cells and photocatalysts. The sol-gel combustion hybrid method can also be used for the large-scale production of nanosized ceramic materials.

Figure 8. Photocurrent-voltage characteristics of solar cells developed by using TiO$_2$ powders synthesized by the sol-gel combustion hybrid method at 500 °C and 600 °C. The measurement was carried out at room temperature with a light intensity of 100 mW/cm², spectral irradiance of AM 1.5, and an active cell area of 0.25 cm².

References

1. Imhof, A.; Pine, D. J. *Nature* **1997**, *389*, 948.
2. Yun, H.-S.; Miyazawa, K.; Zhou, H. S.; Honma, I.; Kuwabara, M. *Adv. Mater.* **2001**, *13*, 1377.
3. Choi, S. Y.; Mamak, M.; Coombs, N.; Chopra, N.; Ozin, G. A. *Adv. Funct. Mater.* **2004**, *14*, 335.
4. Zhong, Z. H.; Han, M. Y. *Angew. Chem. Int. Ed.* **2005**, *44*, 3466.
5. Alexandridis, P.; Athanassiou, L. V.; Hatton, T. A. *Langmuir* **1995**, *11*, 2442.
6. Jing, L.; Sun, X.; Shang, J.; Cai, W.; Xu, Z.; Du, Y.; Fu, H. *Sol. Energy Mater. Sol. Cells* **2003**, *79*, 133.
7. Marple, B. R.; Lima, R. S.; Li, H.; Khor, K. A. *Key Eng. Mater.* **2006**, *309*, 739.
8. Petrella, A.; Tamborra, M.; Cozoli, P. D.; Curri, M. L.; Striccoli, M.; Cosma, P.; Fariola, G. M.; Naso, F.; Agostiano, A. *Thin Solid Films* **2004**, *451*, 64.
9. Degussa Technical Bulletin *Pigments*; 1990; Vol 56, p 13.
10. Ranga Rao, A.; Dutta, V. *Sol. Energy Mater. Sol. Cells* **2007**, *91*, 1075.
11. Montoya, I. A.; Viveros, T.; Dominguez, J. M.; Canales, L. A.; Shifter I. *Catal. Letters* **1992**, *15*, 207.
12. Ding, X.-Z.; Qi, Z.-Z.; He, Y. Z. *J. Mater. Sci. Lett.* **1995**, *14*, 21.
13. Ohtani, B.; Nishimoto, S.-I. *J. Phys. Chem.* **1993**, *97*, 920.
14. Ohtani, B.; Zhang, S.-W.; Nishimoto, S.-I.; Kagiya, T. *J. Photochem. Photobiol. A Chem.* **1992**, *64*, 223.
15. Bischoff, B. L.; Anderson, M. A. *Chem. Mater.* **1995**, *7*, 1772.
16. Wang, C. C.; Ying, J. Y. *Chem. Mater.* **1999**, *11*, 3113.
17. Maslow, V. M.; Neganov, A. S.; Borovinskaya, I. P.; Merzhanov, A. G. *Fiz. Goren. Vzryva* **1978**, *14*, 73.
18. Han, C.-H.; Gwak, J.; Han, S.-D.; Khatkar, S. P. *Materials Letters* **2007**, *61*, 1701.
19. Chen, W.; Sun, X.; Cai, Q.; Weng, D.; Li, H. *Electrochemistry Communications* **2007**, *9*, 382.
20. Nazeeruddin, M. K.; Kay, A.; Rodicio, I.; Humphry-Baker, R.; Muller, E.; Liska, P.; Vlachopoulos, N.; Gratzel, M. *J. Am. Chem. Soc.* **1993**, *115*, 6382.